

Role of remote Coulomb scattering on the hole mobility at cryogenic temperatures in SOI p-MOSFETs

Xian-Le Zhang(张先乐), Peng-Ying Chang(常鹏鹰), Gang Du(杜刚), Xiao-Yan Liu(刘晓彦)

Citation: Chin. Phys. B . 2020, 29(3): 038505 . **doi:** 10.1088/1674-1056/ab6966
Journal homepage: http://cpb.iphy.ac.cn; http://iopscience.iop.org/cpb

What follows is a list of articles you may be interested in

Negative gate bias stress effects on conduction and low frequency noise characteristics in p-type poly-Si thin-film transistors

Chao-Yang Han(韩朝阳), Yuan Liu(刘远), Yu-Rong Liu(刘玉荣), Ya-Yi Chen(陈雅怡), Li Wang(王黎), Rong-Sheng Chen(陈荣盛)

Chin. Phys. B . 2019, 28(8): 088502 . **doi:** 10.1088/1674-1056/28/8/088502

Design and fabrication of 10-kV silicon-carbide p-channel IGBTs with hexagonal cells and step space modulated junction termination extension

Zheng-Xin Wen(温正欣), Feng Zhang(张峰), Zhan-Wei Shen(申占伟), Jun Chen(陈俊), Ya-Wei He(何亚伟), Guo-Guo Yan(闫果果), Xing-Fang Liu(刘兴昉), Wan-Shun Zhao(赵万顺), Lei Wang(王雷), Guo-Sheng Sun(孙国胜), Yi-Ping Zeng(曾一平)

Chin. Phys. B . 2019, 28(6): 068504 . **doi:** 10.1088/1674-1056/28/6/068504

Heavy ion induced upset errors in 90-nm 64 Mb NOR-type floating-gate Flash memory

Jin-Shun Bi(毕津顺), Kai Xi(习凯), Bo Li(李博), Hai-Bin Wang(王海滨), Lan-Long Ji(季兰龙), Jin Li(李金), Ming Liu(刘明)

Chin. Phys. B . 2018, 27(9): 098501 . **doi:** 10.1088/1674-1056/27/9/098501

Physics-based analysis and simulation model of electromagnetic interference induced soft logic upset in CMOS inverter

Yu-Qian Liu(刘彧千), Chang-Chun Chai(柴常春), Yu-Hang Zhang(张宇航), Chun-Lei Shi(史春蕾), Yang Liu(刘阳), Qing-Yang Fan(樊庆扬), Yin-Tang Yang(杨银堂)

Chin. Phys. B . 2018, 27(6): 068505 . **doi:** 10.1088/1674-1056/27/6/068505

Degradation of current-voltage and low frequency noise characteristics under negative bias illumination stress in InZnO thin film transistors

Li Wang(王黎), Yuan Liu(刘远), Kui-Wei Geng(耿魁伟), Ya-Yi Chen(陈雅怡), Yun-Fei En(恩云飞)

Chin. Phys. B . 2018, 27(6): 068504 . **doi:** 10.1088/1674-1056/27/6/068504

Role of remote Coulomb scattering on the hole mobility at cryogenic temperatures in SOI p-MOSFETs*

Xian-Le Zhang(张先乐), Peng-Ying Chang(常鹏鹰)†, Gang Du(杜刚), and Xiao-Yan Liu(刘晓彦)‡

Institute of Microelectronics, Peking University, Beijing 100871, *China*

(Received 13 November 2019; revised manuscript received 24 December 2019; accepted manuscript online 9 January 2020)

The impacts of remote Coulomb scattering (RCS) on hole mobility in ultra-thin body silicon-on-insulator (UTB SOI) p-MOSFETs at cryogenic temperatures are investigated. The physical models including phonon scattering, surface roughness scattering, and remote Coulomb scatterings are considered, and the results are verified by the experimental results at different temperatures for both bulk (from 300 K to 30 K) and UTB SOI (300 K and 25 K) p-MOSFETs. The impacts of the interfacial trap charges at both front and bottom interfaces on the hole mobility are mainly evaluated for the UTB SOI p-MOSFETs at liquid helium temperature (4.2 K). The results reveal that as the temperature decreases, the RCS due to the interfacial trap charges plays an important role in the hole mobility.

Keywords: remote Coulomb scattering, hole mobility, cryogenic temperatures, UTB SOI p-MOSFETs

PACS: 85.30.Tv, 73.40.Qv **DOI:** 10.1088/1674-1056/ab6966

1. Introduction

The CMOS-compatible qubits in silicon[1–8] bring increased interest in cryogenic CMOS (cryo-CMOS) electronics, which provides the best choice for realizing the high level of integration to manipulate a large number of qubits reliably. Under this background, the ultra-thin body silicon-on-insulator (UTB SOI) technology offers an attractive platform to develop a scalable and hybrid quantum computing system.[9–12] Enhanced analog/digital performance of 28 nm UTB SOI technology down to liquid helium temperature (4.2 K) for quantum computing has been demonstrated experimentally.[13,14] However, the design of CMOS qubit-control circuits at cryogenic temperatures is a difficult task, since the physical modeling of cryogenic temperature MOSFETs operation is not so fully developed due to the sophisticated physics at 4.2 K compared to room temperature.[15–19] Thus, the cryo-CMOS device modeling and simulation down to 4.2 K are not adequate yet.

The transport property of carriers is essential to modeling[20,21] and simulation[22,23] of the MOSFETs.[24–27] There has been extensive research into the surface roughness scattering limited mobility,[28,29] while few attention has been paid to the impacts of remote Coulomb scattering on the hole mobility at cryogenic temperatures. Furthermore, the density of interface trap charge increases evidently as the temperature decreases,[30] which can seriously affect the device performance. Therefore, in this work, we aim at investigating the impacts of remote Coulomb scattering. The temperature dependence of the hole mobility in UTB SOI p-MOSFETs from room temperature down to liquid helium temperature (300–4.2 K) is comprehensively studied by considering the phonon scattering, surface roughness scattering, and especially remote Coulomb scattering arising from both the front and bottom interfacial trap charges.

This work is arranged as follows. Section 2 shows the details of our method and verification for both bulk (from 300 K to 30 K) and UTB SOI (300 K and 25 K) devices to evaluate the transport property of UTB SOI p-MOSFETs at cryogenic temperatures. In Section 3, we firstly analyze the influences of the oxide trap charges from the front and bottom interfaces independently, and then study their combined contributions to the total hole mobility at 4.2 K.

2. Simulation method and verification

Figure 1 shows the gate stack of the UTB SOI p-MOSFETs structure in the simulations. The silicon channel is assumed to be undoped. The valence band structure accounting for quantum mechanical confinement is computed by solving the six-band $k \cdot p$ Schrödinger and Poisson equations in a self-consistent way.[31–33] The momentum relaxation time (MRT) approximation and the Kubo–Greenwood formula are used to calculate the hole mobility.[34,35] For the physical modeling of the hole mobility, the following scattering mechanisms are considered: nonpolar acoustic phonon (AP) and optical phonon (OP) scatterings, surface roughness (SR) scattering, and remote Coulomb scattering (RCS). For the nonpolar acoustic, optical phonon scatterings, and surface roughness scattering, their corresponding scattering models are detailed

*Project supported by the National Natural Science Foundation of China (Grant Nos. 61674008, 61421005, and 61804003), the National Key Research and Development Program of China (Grant No. 2016YFA0202101), and the China Postdoctoral Science Foundation (Grant Nos. 2018M630034 and 2019T120017).

†Corresponding author. E-mail: pychang@pku.edu.cn

‡Corresponding author. E-mail: xyliu@ime.pku.edu.cn

© 2020 Chinese Physical Society and IOP Publishing Ltd

described in Refs. [34,35]. Unless otherwise stated, Table 1 lists the key structure and scattering parameters in the simulations.

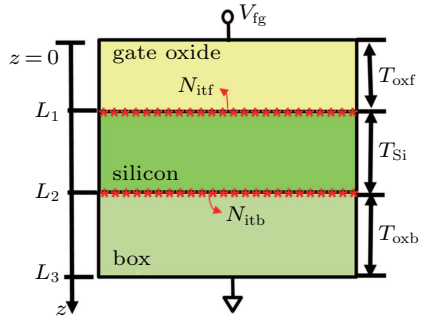


Fig. 1. The gate stack structure of the UTB SOI p-MOSFETs in the simulations, where external charge centers in the front and bottom interfaces are illustrated.

Table 1. Key structure and scattering parameters in the simulations.

Parameters	Values
Surface/channel orientation	(100)/[100]
EOT	0.5 nm
C_t	0.5
Surface correlation length (Λ)	2.85 nm[a], 1.6 nm[b]
Surface average height (Δ)	0.55 nm[a], 0.4 nm[b]
Acoustic deformation potential (D_{ac})	7.12 eV[c], 9.65 eV[d]
Optical deformation potential (DK)	13.241×10^8 eV/cm[e]
Optical phonon energy ($\hbar\omega$)	65 meV[f]

[a]SR parameters for fitting the measured mobility of bulk Si devices in Ref. [39]; [b]SR parameters for fitting the measured mobility of UTB SOI devices in Ref. [43]; [c]acoustic deformation potential D_{ac} for bulk Si devices from Ref. [45]; [d]acoustic deformation potential D_{ac} for UTB SOI devices from Ref. [45]; [e]optical deformation potential for both bulk and UTB SOI devices from Ref. [44]; [f]optical phonon energy for both bulk and UTB SOI devices from Ref. [46].

For RCS, the calculation of MRT for hole inversion corresponding to different subbands is very complicated.[34] According to our calculations, the RCS matrix element for the intersubband transitions in the same valley is at least two orders of magnitude smaller than the intrasubband matrix element. As the temperature decreases to 4.2 K, the matrix element for the intersubband transitions can be completely ignored. Thus, compared to the scattering rate of the intrasubband transitions, the intersubband scattering rate in the same valley can almost be negligible.[47] In this work, only intrasubband scattering is considered, just the same as in Refs. [34,36–38]. This RCS model simultaneously includes the effects of all the following points: (i) distribution of external charged centers, (ii) carrier distribution in the inversion layer, (iii) charged centers' correlation, (iv) image charges, (v) screening of charged centers by the inversion mobile carriers. The MRT for RCS[25] of the i-th subband is given by

$$\frac{1}{\tau^i_{\mathrm{RCS}}} = \sum_t \frac{N_t}{2\pi\hbar}\int_0^{2\pi} k_v(E,\theta+\beta)\frac{\mathrm{d}k_v(E,\theta+\beta)}{\mathrm{d}E} \times \left[e^2\left(1-\frac{2C_tJ_1(QR_t)}{QR_t}\right)\times\left|M^i_t(Q,z_t)\right|^2\right]\mathrm{d}\theta,$$

where $Q=|k-k'|$, k and k' represent the electron wave vectors before and after scattering, respectively, and θ is the scattering angle between the initial k and final k' states. The external charges' distribution is modeled as two-dimensional (2D) sublayers parallel to the semiconductor–insulator interface. The external charges' centers of a sublayer are at plane $z=z_t$ ($0\le z_t\le T_{\mathrm{oxf}}$ or $T_{\mathrm{oxf}}+T_{\mathrm{Si}}\le z_t\le T_{\mathrm{oxf}}+T_{\mathrm{Si}}+T_{\mathrm{oxb}}$) and the area density is represented by N_t. Here, T_{Si} is the silicon channel thickness. T_{oxf} and T_{oxb} are the front and bottom buried oxide thicknesses, respectively. In this work, we mainly investigate the external charges at the front oxide/Si interface (N_{itf}) and bottom Si/box interface (N_{itb}), as shown in Fig. 1. J_1 is the first-order Bessel function. $R_t=\Gamma(3/2)\times1/(2(\pi N_t)^{0.5})$, where $\Gamma(3/2)$ is the gamma function. The charged centers' correlation is also considered, and their degree of correlation is indicated by a parameter C_t. $C_t=0$ means the charges distribution is completely random, while $C_t=1$ refers to the completely uniform distribution of the charges. In this work, $C_t=0.5$ is used. The matrix element $|M^i_t(Q,z_t)|$ presents the interaction between carriers in the i-th subband at $z=z_t$ plane, and is given by

$$\left|M^i_t(Q,z_t)\right| = \int_0^{L_3}\mathrm{d}z\varphi(Q,z,z_t)g_i(z)\times g_i(z),$$

where $g_i(z)$ is the wave function in the i-th subband. The Fourier transform of the scattering potential perturbations $\varphi(Q,z,z_t)$ is

$$\varphi(Q,z,z_t) = eG_Q(z,z_t) - 2\varepsilon_{\mathrm{sc}}\sum_i SS(i)\int_0^{L_3}\mathrm{d}z_1G_Q(z,z_1)g_i(z_1) \times\int_0^{L_3}\mathrm{d}z_2\varphi(Q,z_2,z_t)g_i(z_2),$$

where $\varepsilon_{\mathrm{sc}}$ refers to the permittivity of the semiconductor. The screening constant SS shown in Ref. [38] has been considered in the long-wavelength limit in this work, just the same as in Ref. [49]. We employ a time-consuming self-consistent procedure to accurately calculate the potential perturbations produced by the external charged centers, which include the dependence of the screening constant on Q. $eG_Q(z,z')$ represents the unscreened case, where $G_Q(z,z')$ has been detailed described in Ref. [37]. In particular, the employed RCS model is valid for bulk, ultrathin double gate (DG), and single gate (SG) silicon-on-insulator devices,[36–38] and can directly take the impacts of temperature into account, which fulfils the needs to study the impacts of RCS on hole mobility at cryogenic temperatures. In this work, the UTB SOI p-MOSFETs operated only in SG mode are considered in all simulations, where the front gate is biased at V_{fg}, and the bottom gate is grounded. The trap charges located at the front and bottom interfaces that

are considered in the following can be treated as a kind of external charges in the above RCS model.

The results shown in Figs. 2(a)–2(c) reproduce well the experimental data of bulk silicon devices from 300 K to 30 K in Ref. [39]. For SR scattering, $\Delta = 0.55$ nm and $\Lambda = 2.85$ nm are adopted by calibration with the experiment. For bulk devices, the trap charges are assumed to be at the front oxide/Si interface, and $N_{\rm itf}$ is set to be 3×10^{10} cm^{-2} at 300 K, 3.0×10^{11} cm^{-2} at 77 K, and a higher value of 4.0×10^{11} cm^{-2} at 30 K, which can be explained by an increase of interface trap states density as the temperature decreases.[30]

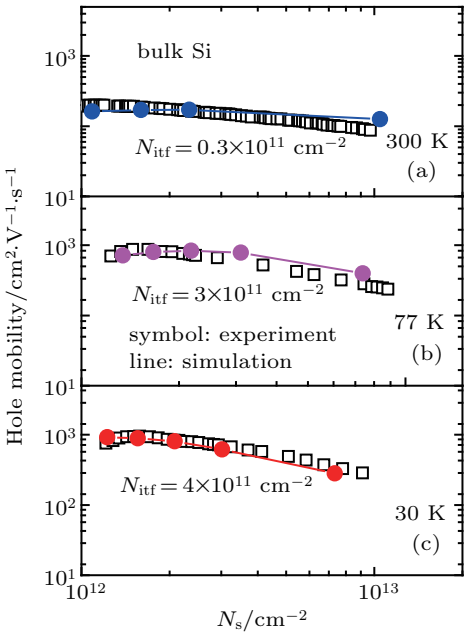


Fig. 2. Calculated hole mobility (lines) versus inversion density at different temperatures: (a) 300 K, (b) 77 K, (c) 30 K. Symbols are for the measured hole mobility.[39] These results verify our simulation method and parameters listed in Table 1 for a wide range of temperatures in the bulk devices.

To verify our method for the UTB SOI p-MOSFETs, we reproduce well the experimental data[43] of 7 nm-thick-body undoped UTB SOI for both 300 K and 25 K, as shown in Fig. 3. Here, the acoustic deformation potential $D_{\rm ac}$ is set to a higher value of $D_{\rm ac} = 9.65$ eV[45] than the value adopted in the bulk silicon devices, in agreement with Ref. [34], which is the reasonable way[48] for the need to reproduce the experimental data for SOI devices. $\Delta = 0.4$ nm and $\Lambda = 1.6$ nm are used for the SR scattering parameters, which are significantly different from those in Fig. 2 as the interface quality strongly depends on the fabrication process. For RCS, the trap charges at both front and bottom interfaces are considered for the UTB SOI devices, where charge density $N_{\rm itf}$ at the front interface can be less than or equal to charge density $N_{\rm itb}$ at the bottom interface.[40–42] Thus, $N_{\rm itf}$ and $N_{\rm itb}$ are respectively set to be 4×10^9 cm^{-2} and 8×10^9 cm^{-2} at 300 K, while much higher values of 3.75×10^{11} cm^{-2} and 3.8×10^{11} cm^{-2} are adopted at 25 K to fit with the experimental data. As mentioned above, this increase of the interface trap density with the decrease of the temperature is consistent with the experiment.[30] As the excellent agreement in Figs. 2 and 3 verifies our physical models and parameters listed in Table 1 for different temperatures, our simulations methods can then be reliably employed to further evaluate the hole mobility down to 4.2 K. Note that the above-mentioned SR and phonon scattering parameters extracted from the UTB SOI device are adopted to the simulations of 7 nm-thick-body undoped UTB SOI p-MOSFETs in the following.

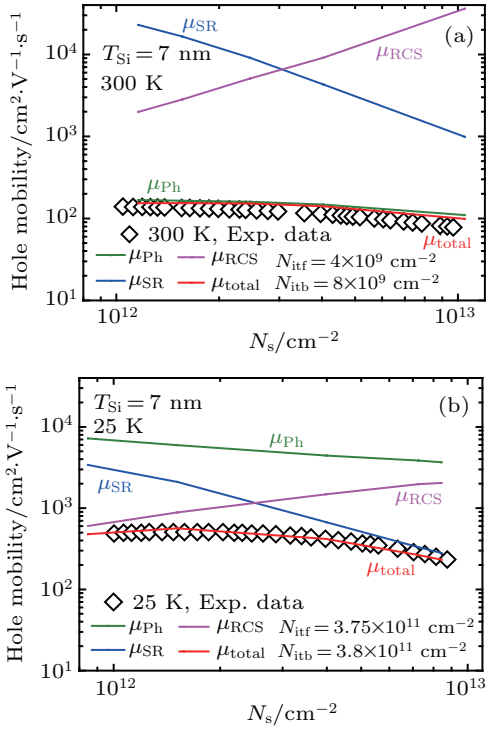


Fig. 3. Calculated hole mobility versus inversion density at (a) 300 K and (b) 25 K for 7 nm-thick-body (100)/[100] UTB SOI p-MOSFETs. Symbols are for the measured hole mobilities.[43] $\Delta = 0.4$ nm and $\Lambda = 1.6$ nm are used for the SR scattering parameters. These results verify our simulation method and parameters listed in Table 1 for a wide range of temperatures in the UTB SOI devices.

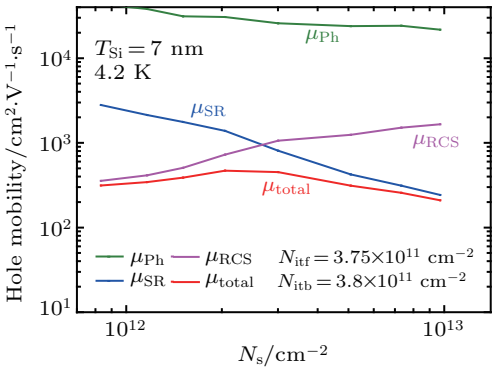


Fig. 4. Calculated hole mobility versus inversion density for 7 nm-thick-body (100)/[100] UTB SOI p-MOSFETs at 4.2 K, where $N_{\rm itf} = 3.75 \times 10^{11}$ cm^{-2} and $N_{\rm itb} = 3.8 \times 10^{11}$ cm^{-2} are adapted here. $\Delta = 0.4$ nm and $\Lambda = 1.6$ nm are used for the SR scattering parameters.

In order to more clearly show the variation of the types of dominant scattering mechanisms from 300 K to 4.2 K, the hole

mobility at 4.2 K is also calculated as shown in Fig. 4. Particularly, the contributions of different scattering mechanisms to the total mobility are also shown in Figs. 3 and 4, revealing that the dominant scattering mechanism is significantly different at different temperatures and different inversion densities. At high temperature, phonon scattering is dominant. However, as the temperature decreases to 4.2 K as shown in Fig. 4, its impact is almost negligible, while RCS and SR scatterings then become the two dominant scattering mechanisms. What is more, since the effect of screening is weak due to the low inversion hole density, RCS has a dominant influence on the hole mobility at low hole density. It should be noted that without considering RCS, the calculated mobility cannot be fitted to the experimental results at low hole density, further suggesting the significance of RCS. On the other hand, SR scattering then has a major impact at high hole density since the screening effect of the inversion hole suppresses the RCS.

3. Results and discussion

3.1. Impacts of the front interface and oxide trap charges

Temperature dependent hole mobilities including the impacts caused by the trap charges at the front SiO_2/Si interface for 7 nm-thick-body (100)/[100] UTB SOI p-MOSFETs are investigated, where $N_{itf} \neq 0$ and $N_{itb} = 0$. Figure 5(a) shows the RCS limited mobility without screening versus temperature (4.2–300 K) with three different values of N_{itf} at $N_s = 2 \times 10^{12}$ cm^{-2}. When the temperature is below 30 K, the unscreened RCS limited mobility tends to be almost constant. However, when the temperature is greater than 30 K, the unscreened RCS limited mobility decreases as the temperature decreases, so the scattering due to the interaction between the trap charges and inversion carriers increases as the temperature decreases. Actually, the RCS rate depends on not only the scatterings due to the interaction between the trap charges and inversion carriers but also the screening by the inversion carrier charges. As the screening constant SS can directly represent the screening effect, we adopt average screening constant SS_{ave} defined as

$$SS_{ave} = \frac{\sum_{i=1}^{N_{sub}} SS(i) \times N(i)}{\sum_{i=1}^{N_{sub}} N(i)},$$

where N_{sub} represents all the subbands, and $N(i)$ and $SS(i)$ are the carrier density and screening constant of the i-th subband, respectively. The trend of parameter SS_{ave} versus temperature at $N_s = 2 \times 10^{12}$ cm^{-2} is plotted in Fig. 5(b). The value of SS_{ave} is larger, the corresponding screening effect is more significant. As the temperature is below 30 K, the average screening effect tends to be small temperature dependent, and this result coincides with the results in Ref. [49]. When the temperature is above 30 K, the average screening effect increases as the temperature decreases. Thus, the screening effect versus temperatures has almost the same trend compared with that of the scattering due to the interaction between the trap charges and inversion carriers. The RCS limited mobility with screening effect versus temperature (4.2–300 K) with three different values of N_{itf} at $N_s = 2 \times 10^{12}$ cm^{-2} is plotted in Fig. 6(a). Obviously, the RCS limited mobility in Fig. 6(a) is the results due to the combined contributions of both the scattering and screening effects mentioned above, which are respectively shown in Figs. 5(a) and 5(b). Thus, for the unscreened one, the scattering due to the interaction between the trap charges and inversion carriers plays a dominant role. However, as for the screened case, the impact of the screening effects by the inversion carrier charge on the RCS limited mobility is more dominant. On the other hand, when N_{itf} increases from 4×10^9 cm^{-2} cm^{-2} to 3.75×10^{11} cm^{-2}, the RCS limited mobility almost proportionally decreases as the change of orders of magnitude of the trap density.

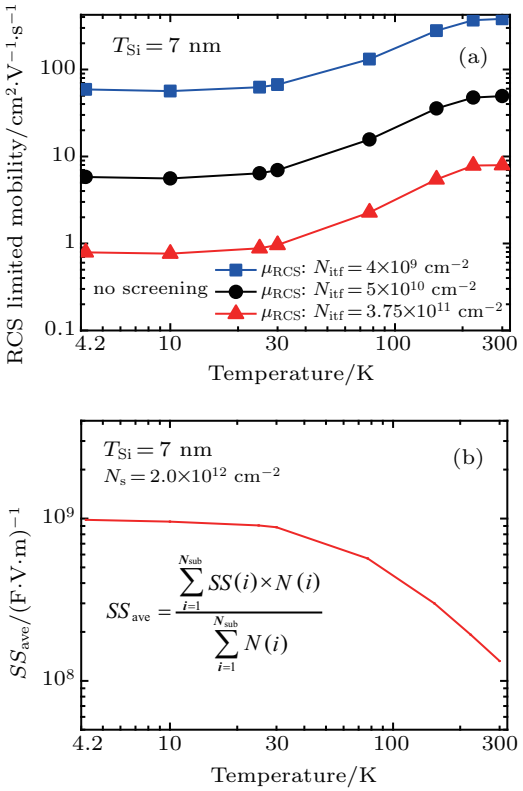


Fig. 5. (a) The RCS limited mobility without screening versus temperature (4.2–300 K) with three different values of N_{itf} at $N_s = 2 \times 10^{12}$ cm^{-2}. (b) The average screening constant SS_{ave} versus temperature at $N_s = 2 \times 10^{12}$ cm^{-2}.

Figure 6(a) also plots the SR and phonon scattering limited mobility versus temperature (4.2–300 K). The phonon limited mobility increases monotonically with decreasing temperature, while the SR scattering limited mobility has almost an opposite temperature dependence. As the temperature decreases, electrons are given less kinetic energy so that they

are more vulnerable to SR scattering, leading to the reduction of the SR limited mobility. However, when the temperature is below 30 K, the SR limited mobility becomes almost temperature independent. Figure 6(b) shows the temperature dependence of the corresponding total hole mobility. For all N_{itf} cases, the hole mobility increases as the temperature decreases. What is more, the hole mobility at 4.2 K is an order of magnitude higher than that at 300 K whatever the trap charge density is. For example, at high N_{itf} of 3.75×10^{11} cm^{-2}, the hole mobility at 4.2 K is 642 cm^2/V·s, and in contrast its value is only 79 cm^2/V·s at 300 K.

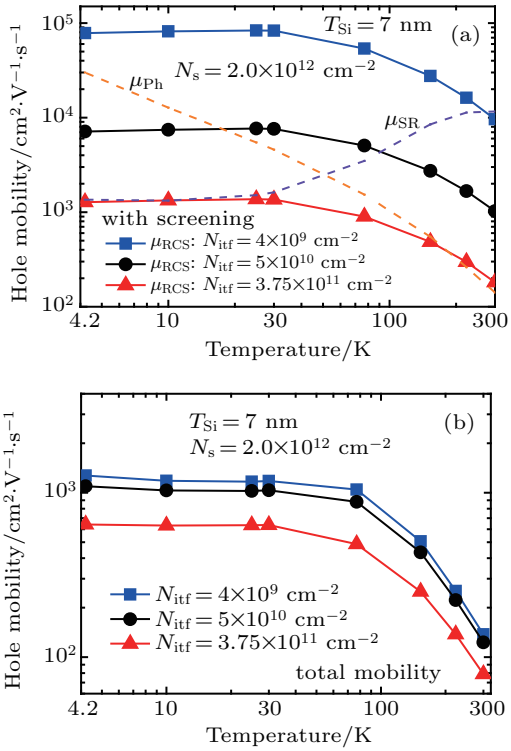


Fig. 6. (a) RCS, SR, and phonon scattering limited mobility and (b) the total hole mobility versus temperature (4.2–300 K) with three different values of N_{itf} at $N_s=2.0\times10^{12}$ cm^{-2}. $\Delta=0.4$ nm and $\Lambda=1.6$ nm are used for the SR scattering parameters.

Compared with the phonon scattering, the RCS and SR scattering have dominant effects on the hole mobility at 4.2 K, and thus the hole mobility is evaluated by considering only RCS (with screening) and SR scattering in all simulations below. Figure 7 shows the calculated hole mobility versus hole inversion density with two N_{itf} taken the experimentally extracted values[16] at 4.2 K. At low hole density ($N_s=8.3\times10^{11}$ cm^{-2}), the total hole mobility is 311 cm^2/V·s and 39 cm^2/V·s for N_{itf} of 8×10^{11} cm^{-2} and 8×10^{12} cm^{-2}, respectively. Thus, the increase of N_{itf} by an order of magnitude can produce a decrease of the total hole mobility by the almost same order of magnitude. However, at high hole density ($N_s=9.7\times10^{12}$ cm^{-2}), the total hole mobility is 209 cm^2/V·s for $N_{itf}=8\times10^{11}$ cm^{-2}. As the value of N_{itf} rises up to 8×10^{12} cm^{-2}, the total hole mobility is reduced to 106 cm^2/V·s. These results suggest that the RCS induced change of the hole mobility becomes smaller at higher hole inversion density due to the stronger screening effect.

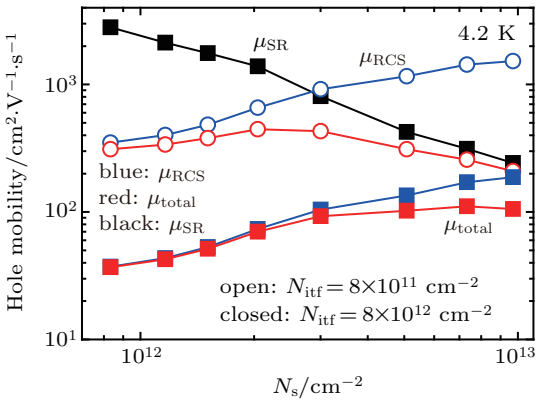


Fig. 7. Calculated hole mobility versus hole inversion density with N_{itf} of 8×10^{11} cm^{-2} and 8×10^{12} cm^{-2} considering RCS and SR scatterings in 7 nm-thick-body (100)/[100] UTB SOI p-MOSFETs at 4.2 K. $\Delta=0.4$ nm and $\Lambda=1.6$ nm are used for the SR scattering parameters.

Additionally, to reveal the impact of the position of the trap charges in the front gate oxide on the hole transport properties, two effective oxide thicknesses (EOT) of 0.5 nm and 1.0 nm are considered with two kinds of trap charges positions ($z_t=0$ and $z_t=T_{oxf}$). Figure 8 plots the calculated mobility versus hole sheet density for the trap charges in two different positions in the front oxide with the same N_{itf} at 4.2 K. If the impacts of the front SiO_2/Si interfacial trap charges are mainly considered ($z_t=T_{oxf}$), the RCS limited mobility difference is very small for different values of EOT. However, for the same EOT case, the RCS limited mobility is decided by the positions of the trap charges. For example, for the EOT = 1 nm case, the trap charges' position of $z_t=0$ (red line) is farther away from the inversion carriers compared with that of $z_t=T_{oxf}$ (blue line), so its corresponding RCS limited mobility (red line) is larger.

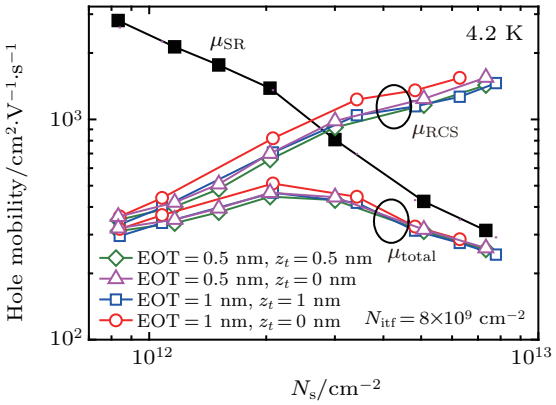


Fig. 8. Calculated mobility versus the hole sheet density for the trap charges in two different positions in the front oxide at 4.2 K. The charges density here is set to be 8×10^{11} cm^{-2}. $\Delta=0.4$ nm and $\Lambda=1.6$ nm are used for the SR scattering parameters.

3.2. Impacts of the bottom interface trap charges

Trap charges at the bottom buried interfaces play a more dominant role in remote Coulomb scatterings compared with

those inside the buried oxide.[40] Thus here we mainly focus on the impacts of trap charges at the bottom interface, where $N_{itf} = 0$ and $N_{itb} \neq 0$. The calculated hole mobility versus hole sheet density with two different N_{itb} for 7 nm-thick-body (100)/[100] UTB SOI p-MOSFETs at 4.2 K is shown in Fig. 9. At low hole density, an order of magnitude increase of N_{itb} also brings an order of magnitude decrease in the hole mobility, as N_{itb} increases from 8×10^{11} cm^{-2} to 8×10^{12} cm^{-2}, which indicates that the impacts of the trap charges at the bottom interface on the mobility become more important. Moreover, at high hole density ($N_s = 9.7 \times 10^{12}$ cm^{-2}), the total hole mobility is 226 cm^2/V·s with $N_{itb} = 8 \times 10^{11}$ cm^{-2}. As the value of N_{itb} reaches up to 8×10^{12} cm^{-2}, the total hole mobility is reduced to 145 cm^2/V·s.

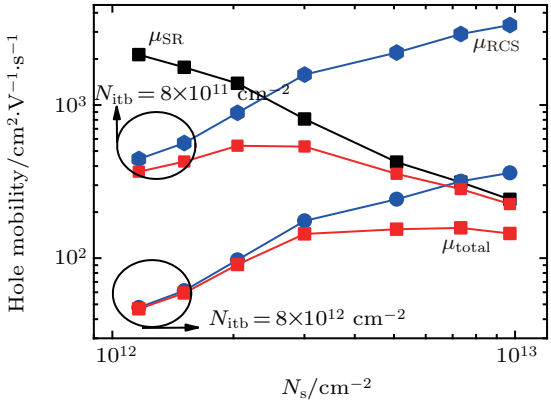


Fig. 9. Calculated hole mobility versus hole inversion density with N_{itb} of 8×10^{11} cm^{-2} and 8×10^{12} cm^{-2} considering RCS and SR scattering in 7 nm-thick-body (100)/[100] UTB SOI p-MOSFETs at 4.2 K. $\Delta = 0.4$ nm and $\Lambda = 1.6$ nm are used for the SR scattering parameters.

3.3. Impact of trap charges at both interfaces on the hole mobility at 4.2 K

For comparison, the hole mobility considering the impacts of both interfaces with N_{itf} and N_{itb} of 8×10^{11} cm^{-2} and 8×10^{12} cm^{-2} for 7 nm-thick-body (100)/[100] UTB SOI p-MOSFETs is plotted in Fig. 10. A pair of numbers (N_{itf}, N_{itb}) (expressed in units of 10^{12} cm^{-2}) is used to represent each curve. For example, curve (8, 0) represents the case of $N_{itf} = 8 \times 10^{12}$ cm^{-2} and $N_{itb} = 0$, curve (0, 8) represents the case of $N_{itf} = 0$ and $N_{itb} = 8 \times 10^{12}$ cm^{-2}, and curve (8, 8) represents the case of $N_{itf} = 8 \times 10^{12}$ cm^{-2} and $N_{itb} = 8 \times 10^{12}$ cm^{-2}. At low hole density (N_s of 8.3×10^{11} cm^{-2}), if RCS is neglected (that is, only SR is considered), the total mobility is about 2805 cm^2/V·s. However, when RCS due to only front interface trap charges is considered, the total mobility is reduced to 311 cm^2/V·s. If the impacts of the front and bottom interface trap charges are simultaneously considered, the total mobility is further reduced to 168.6 cm^2/V·s. The values of mobility under two interfacial trap charge densities for both weak and strong inversion are detailed listed in Table 2. Apparently, the trap charge at the front interface has more significant impacts on the mobility than that at the bottom interface at high hole density, as the corresponding carrier centroid distribution is nearer the front interface. However, at low hole density, it is clear that the trap charge of the bottom interface has comparable impacts on the mobility to that of the front interface, as the corresponding carrier centroid distribution tends to be symmetrical with respect to both the front and bottom interfaces. Therefore, as the temperature is reduced to 4.2 K, the impacts of the trap charges at both interfaces on the mobility should be considered simultaneously in thin UTB SOI devices.

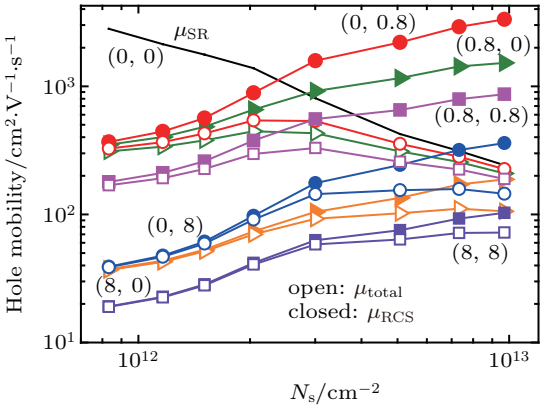


Fig. 10. Comparison of calculated hole mobility considering RCS and SR scattering in 7 nm-thick-body (100)/[100] UTB SOI p-MOSFETs at 4.2 K with both interfaces having the same trap charges density. The charged center densities at the front (N_{itf}) and bottom (N_{itb}) interfaces are represented by a pair of numbers in the units of 10^{12} cm^{-2}. $\Delta = 0.4$ nm and $\Lambda = 1.6$ nm are used for the SR scattering parameters.

Table 2. Hole mobility (in cm^2/V·s) at different N_s for different (N_{itf}, N_{itb}) (in 10^{12} cm^{-2}).

N_s/cm^{-2}	(0,0)	(0.8,0)	(0,0.8)	(0.8,0.8)	(8,0)	(0,8)	(8,8)
	μ_{sr}	μ_{rcs}/μ_{sr+rcs}	μ_{rcs}/μ_{sr+rcs}	μ_{rcs}/μ_{sr+rcs}	μ_{rcs}/μ_{sr+rcs}	μ_{rcs}/μ_{sr+rcs}	μ_{rcs}/μ_{sr+rcs}
8.3×10^{11}	2804	350/311	368/326	179/169	37/37	39/39	19/19
9.7×10^{12}	242	1524/209	3326/226	867/189	187/106	360/145	103/72

4. Conclusion

The impacts of remote Coulomb scattering on hole mobility in UTB SOI p-MOSFETs at cryogenic temperatures (from 300 K to 4.2 K) are evaluated. At 4.2 K, phonon scattering can be almost negligible, and RCS and SR scattering are the two dominant scattering mechanisms. RCS has a dominant effect on mobility at low hole density, while SR has a major impact on the mobility at high hole density. The trap charges at the bottom buried interface has comparable important impacts on the total mobility to that at the front oxide/Si interface in thin

body thickness UTB SOI p-MOSFETs at 4.2 K. Particularly, the hole mobility at 4.2 K is higher than that at 300 K. The results are helpful for modeling and simulation of CMOS circuits at cryogenic temperatures.

References

[1] Pla J J, Tan K Y, Dehollain J P, Lim W H, Morton J J L, Jamieson D N, Dzurak A S and Morello A 2012 *Nature* **489** 541

[2] Elzerman J M, Hanson R, Willems v B L H, Witkamp B, Vandersypen L M K and Kouwenhoven L P 2004 *Nature* **430** 431

[3] Zhang J F, Mao W, Zhang J C and Hao Yue 2008 *Chin. Phys. B* **17** 2689

[4] Veldhorst M, Hwang J C C, Yang C H, Leenstra A W, Ronde B D, Dehollain J P, Muhonen J T, Hudson F E, Itoh K M, Morello A and Dzurak A S 2014 *Nat. Nanotechnol.* **9** 981

[5] Maurand R, Jehl X, Kotekar-Patil D, Corna A, Bohuslaveskyi H, Lavieville R, Hutin L, Barraud S, Vinet M, Sanquer M and Franceschi S D 2016 *Nat Commun.* **7** 13575

[6] Boeuf F, Jehl X, Sanquer M and Skotnicki T 2003 *IEEE Trans. Nano.* **2** 144

[7] Liu Y, Liu K, Chen R S, Liu Y R, En Y F, Li B and Fang W X 2017 *Chin. Phys. Lett.* **34** 18501

[8] Zheng J J, Wang Y R, Yu K H, Xu X X, Sheng X X, Hu E T and Wei W 2018 *Acta Phys. Sin.* **67** 118502 (in Chinese)

[9] Beckers A, Jazaeri F, Bohuslavskyi H, Hutin L, Franceschi S D and Enz C 2019 *Solid-State Electron.* **159** 106

[10] Franceschi S D, Hutin L, Maurand R, Bourdet L, Bohuslavskyi H, Corna A, Kotekar-Patil D, Barraud S, Jehl X, Niquet Y M, Sanquer M and Vinet M 2017 *2017 IEEE IEDM Tech. Dig. America*, p. 13.4.1

[11] Gopi Krishna S, Sarvesh D and Pramod Kumar T 2015 *Chin. Phys. B* **24** 108505

[12] Ya-Mei D, Wei-Hua H, Yang-Yan G, Xiao-Song Z, Xiao-Di Z, Xin-Yu W and Fu-Hua Yang 2019 *Chin. Phys. B* **28** 066804

[13] Bohuslavskyi H, Barraud S, Casse M, Barral V, Bertrand B, Hutin L, Arnaud F, Galy P, Sanquer M, Franceschi S D and Vinet M 2017 *Silicon Nan electronics Workshop (SNW)*, June, 2017 Japan, p. 143

[14] Galy P, Camirand Lemyre J, Lemieux P, Arnaud F, Drouin D and Pioro-Ladriere A M 2018 *J. Electron. Dev. Soc.* **6** 594

[15] Incandela R M, Song L, Homulleet H, Charbon E, Vladimirescu A and Sevastiano F 2018 *J. Electron. Dev. Soc.* **6** 996

[16] Beckers A, Jazaeri F, Bohuslavskyi H, Hutin, L, De Franceschi S and Enz C 2018 *Joint International EUROSOI Workshop and International Conference on Ultimate Integration on Silicon (EUROSOI-ULIS)*, March, 2018 p. 1

[17] Jazaeri F, Beckers A, Tajalli A and Sallese J M 2019 *International Conference Mixed Design of Integrated Circuits and Systems (MIXDES)*, August 2019 p. 15

[18] Zhao X S, Han W H, Guo Y Y, Dou Y M and Yang F H 2018 *Chin. Phys. B* **27** 097310

[19] Gao Z Z, Hou P F, Guo H X, Li B, Song H J, Wang J B and Zhong X L 2019 *Acta Phys. Sin.* **68** 048501 (in Chinese)

[20] Wu H, Duan B X, Yang L Y and Yang Y T 2019 *Chin. Phys. B* **28** 027302

[21] Chen W Z, Huang Y, He L J, Han Z S and Huang Y 2018 *Chin. Phys. B* **27** 088501

[22] Shao Y and Ding S J 2018 *Acta Phys. Sin.* **67** 098502 (in Chinese)

[23] Wen Z X, Zhang F, Shen Z W, Chen J, He Y W, Yan G G, Liu X F, Zhao W S, Wang L, Sun G S and Zeng Y P 2019 *Chin. Phys. B* **28** 068504

[24] Han T C, Zhao H D and Peng X C 2019 *Chin. Phys. B* **28** 047302

[25] Zhou X Y, Lv Y J, Tan X, Wang Y G, Song X B, He Z Z, Zhang Z R, Liu Q B, Han T T, Fang Y L and Feng Z H 2018 *Acta Phys. Sin.* **67** 178501 (in Chinese)

[26] Yang W, Song J J and Ren Y 2018 *Acta Phys. Sin.* **67** 198502 (in Chinese)

[27] Mao S J, Zhu Z Y, Wang G L, Zhu H L, Li J F and Zhao C 2016 *Chin. Phys. Lett.* **33** 118502

[28] Gámiz F 2004 *Semicond. Sci. Technol.* **19** 113

[29] Zhao Y, Takenaka M and Takagi S 2009 *Electron. Dev. Lett.* **30** 987

[30] Hafez I M, Ghibaudo G and Balestra F 2018 *J. Appl. Phys.* **67** 1950

[31] Chang P Y, Liu X Y, Zeng L and Du G 2015 *Solid-State Electron.* **113** 68

[32] Chang P Y, Liu X Y, Zeng L, Wei K L and Du G 2015 *Trans. Electron. Devices* **62** 947

[33] Fischetti M V, Ren Z, Solomon P M, Yang M and Rim K 2003 *J. Appl. Phys.* **94** 1079

[34] Esseni D, Palestri P and Selmi L 2011 *Nanoscale MOS Transis-tors: Semi-Classical Transport and Applications* (Cambridge: Cambridge University Press) p. 156

[35] Chang P Y, Liu X Y, Di S Y and Du G 2017 *Trans. Electron. Devices* **64** 1053

[36] Gámiz F, Roldan J B, Carceller J E and Cartujo P 2003 *Appl. Phys. Lett.* **82** 3151

[37] Gámiz F, Jimenez-Molinos F, Roldan J B and Cartujo-Cassinello P 2002 *Appl. Phys. Lett.* **80** 3835

[38] Gámiz F, López-Villanueva J A, Jiménez-Tejada J A, Melchor I and Palma A 1994 *J. Appl. Phys.* **75** 924

[39] Takagi S, Toriumi A, Iwase M and Tango H 1994 *IEEE Trans. Electron. Devices* **41** 2357

[40] Koga J, Takagi S and Toriumi A 2002 *IEEE Trans. Electron. Devices* **49** 1042

[41] Schmidt M, Mollenhauer T, Gottlob H D B, Wahlbrink T, Efavi J K, Ottaviano L, Cristoloveanu S, Lemme M C and Kurz H 2005 *Microelectron. Eng.* **82** 497

[42] Esseni D, Abramo A, Selmi L and Sangiorgi E 2003 *IEEE Trans. Electron. Devices* **50** 2445

[43] Uchida K, Watanabe H, Koga J, Kinoshita A and Takagi S 2003 *International Conference on Simulation of Semiconductor Processes & Devices 2003* p. 8

[44] Fsichetti M V and Laux S E 1996 *J. Appl. Phys.* **80** 2234

[45] Wang E X, Matagne P, Shifren L, Obradovic B, Kotlyar R, Cea S, Stettler M and Giles M D 2006 *IEEE Trans. Electron. Devices* **53** 1840

[46] Oberhuber R, Zandler G and Vogl P 1998 *Phys. Rev. B* **58** 9941

[47] Yokoyama K and Hess K 1986 *Phys. Rev. B* **33** 5595

[48] Koba S, Ishida R, Kubota Y, Tsuchiya H, Kamakura Y, Mori N and Ogawa M 2014 *J. J. Appl. Phys.* **53** 114301

[49] Stern F 1980 *Phys. Rev. Lett.* **44** 1469